The phase structure of SPUs was characterized by synchrotron SAXS. SAXS was measured at BL10C at Photon Factory, KEK, Tsukuba, Japan. Figure 6 (a) shows the dependence of corrected intensity on scattering vector of PCL(1250)(X)PDO. q is defined as $4\pi\sin\theta/\lambda$, where θ and λ are Bragg angle and wavelength of X-ray, respectively. Lorentzian factor was corrected by multiplying q^2 to the intensity. A large peak observed at q=ca.0.27 nm^{-1} is attributed to the long period between PCL crystallite. Even the PCL(1250)(100)PDO without hard segment component, the long period was clearly observed. The intensity of this peak decreased with an increase in hard segment fraction and finally disappeared for the LDI-PDO homopolymer. The scattering peak corresponding to the distance between hard segment domains was not observed in SPUs. This can be explained either by the partial phase mixing of hard and soft segments or the absence of the difference in electron density between hard and soft segments. The structure model of PCL(1250)(X)PDO based on above mentioned characterization is depicted in Figure 4(b). PCL formed folded lamellar crystal between hard segment domains. Fairy large amount of amorphous PCL might be present in the soft segment phase. Since the PCL form the large crystallite, PCL(1250)(X)PDO forms three phase structure consists of glassy hard segment, amorphous PCL and crystalline PCL phase.

The mechanical properties of SPUs were investigated by stress-strain measurement. Figure 7 shows the stress-strain curves for SPUs with various PCL fractions. Below T_g of hard segment (302K) and T_m of PCL(283-320K), both hard segment and crystalline PCL phase can act as crosslink at low elongation. However, the PCL crystallite is easily deformed at this temperature, the yielding was observed at low elongation region. Beyond the yielding point, the amorphous PCL phase with low T_g act as rubber elastic component. On the other hand, the elongation at break increased with an increase in soft segment fraction.

Degradation Behavior. The degradation characteristics of a series of SPUs were evaluated. Figure 8 shows the change in weight with time after immersion in Tris-buffer solution at 310 K for SPUs with various soft segment contents. At 310 K, PCL phase in SPU might be melted and the hard segment is in leather like state. The magnitude of degradation in SPUs was increased with an increase in the soft segment fraction. This is because the soft segment has the hydrolyzable ester linkages and the ester linkages are susceptible to hydrolysis compared with the urethane linkages. On the other hand, PCL-LDI soft segment homopolymer showed small magnitude of degradation. This can be ascribed to the presence of PCL crystallites at 310 K.

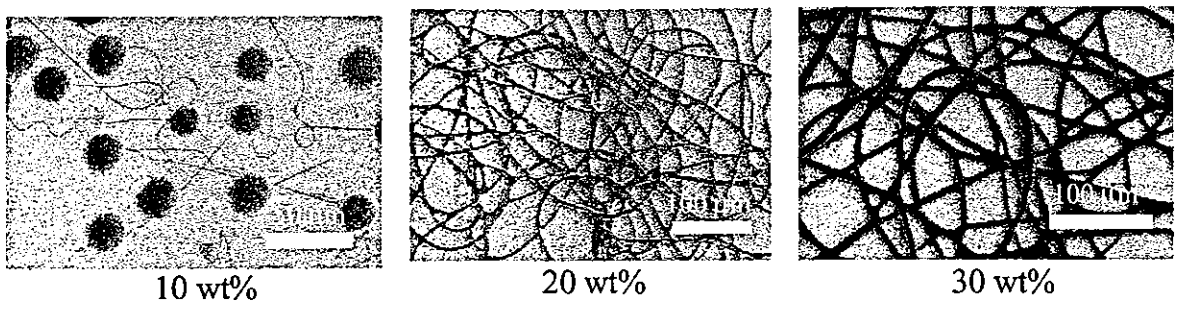

Figure 9 FE-SEM images of microstructure of PCL(1250)(80)PDO ESD microfibers prepared at 10-30 wt% chloroform solution under voltage of 12 kV.

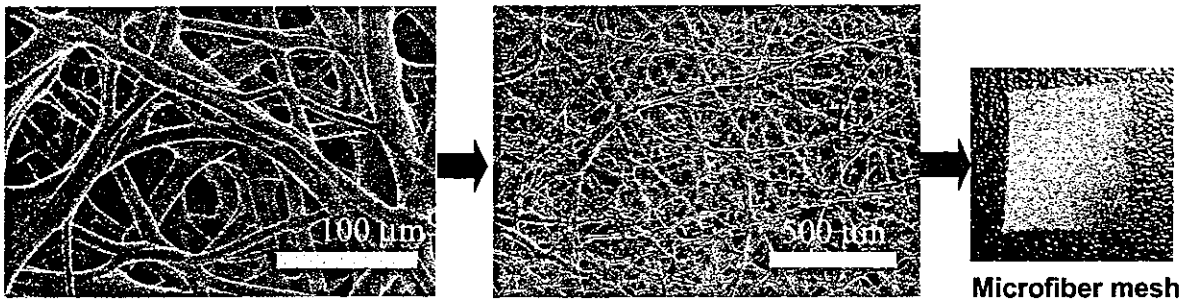

Figure 10 FE-SEM images of SPU microfiber mesh prepared by ESD.

Electro-spray Deposition. In ESD experiment, morphological change of the electrospray deposited microstructure is expected when the concentration of polymer solutions was changed. Figure 9 shows FE-SEM images of PCL(1250)(80)PDO ESD microfibers deposited from 10-30wt% solution under 12 kV. FE-SEM images showed that a mixture of large beads and fibers were formed by ESD at 10 wt% PCL(1250)(80)PDO solution under voltage of 12 kV. In contrast, fine fibers were formed at 20 wt% and 30wt% PCL(1250)(80)PDO solution. The average diameters of the fibers prepared at 10wt%, 20wt%, and 30wt% were 1.0 μm, 7.5 μm, and 7.7 μm, respectively. It was shown that higher concentration of solution favored to form uniform fibers without beads-like structure. This is because the critical viscosity in solution needs to be exceeded in order to fabricate fibers. Below this viscosity chain entanglements are insufficient to stabilize the jet, leading to spraying of droplets. A repeated deposition of microfiber with transverse movement of substrate gives mesh of SPU microfibers. Figure 10 shows FE-SEM images of PCL(1250)(80)PDO microfiber mesh prepared from 35 wt% solution under 12 kV with flow rate of 1 ml h^{-1}. The average diameters

of the fibers was 11.6 μm As shown in Figure 10, self-standing microfiber mesh with high porosity was successfully obtained from ESD of SPU.

Conclusion

Novel biodegradable segmented polyurethanes were prepared from lysine-based diisocyanate, PCL, and PDO chain extender. DSC, dynamic viscoelastic measurements, and small-angle X-ray scattering experiment revealed that the SPU has amorphous PCL, crystalline PCL, and glassy hard segment structure. Degradation rate of SPUs was confirmed by the exposure of SPU film to buffer solution. Microfibers and microfiber mesh of SPU were successfully prepared by electro-spray deposition.

Acknowledgement

This work was partially supported by a Grant-in-Aid for Scientific Research from Ministry of Health, Labor and Welfare (MHLW) of Japan, a Grant-in-Aid for Scientific Research (A)(2) (No.15205028) from Japan Society for the Promotion of Science and P&P, Green Chemistry, of Kyushu University. The SEM observation was made using FE-SEM at the Kyushu University Station-II for collaborative research.

References

[1] K. A. Athanasiou, G. G. Niederauer and C. M. Agrawal, *Biomaterials*, **17**, 93(1996).

[2] P. Bruin, G. J. Veenstra, A. J. Nijenhuis, A. J. Pennings, *Makromol. Chem. Rapid Commun.*, **9**, 589(1988).

[3] J. M. Deitzel, J. Kleinmeyer, D. Harris, N. C. Beck Tan, *Polymer*, **42**, 261(2001).

[4] G. A. Skarja and K. A. Woodhouse, *J. Biomater. Sci. Polymer Edn.*, **13**, 391(2002).

[5] D. J. Lyman, *J. Polym. Sci.*, **45**, 49(1960).

[6] A. Takahara, J. Tashita, T. Kajiyama, M. Takayanagi, W. J. MacKnight, *Polymer*, **26**, 987(1985).

[7] A. Takahara, K. Takahash, T. Kajiyama, *J. Biomater. Sci., Polym. Ed.*,**5**, 183 (1993).

[8] S. Kidoaki, I.K. Kwon, T. Matsuda, *Biomaterials*, **26**, 37(2005).

TISSUE ENGINEERING
Volume 9, Number 6, 2003

System-Engineered Cartilage Using Poly(*N*-isopropylacrylamide)-Grafted Gelatin as *in Situ*-Formable Scaffold: *In Vivo* Performance

SHINICHI IBUSUKI, M.D.,[1,2] YUKIHIDE IWAMOTO, M.D., Ph.D.,[2] and TAKEHISA MATSUDA, Ph.D.[1]

ABSTRACT

Our previous study showed that cartilaginous tissue can be engineered *in vitro* with articular chondrocytes and poly(*N*-isopropylacrylamide)-grafted gelatin. This short-term *in vivo* study for cartilage repair was performed to screen a candidate method for a long-term study. In our previous *in vitro* study, however, two potential problems with the tissue-engineered cartilage were identified: (1) leakage of the transplant due to temperature decline and (2) concave deformation of transplant due to compressive loading. To solve these problems, we investigated in this study the usefulness of suturing with two different covering materials (periosteum or collagen film) and preculturing an engineered tissue for 2 weeks. PNIPAAm–gelatin-based engineered cartilage samples were evaluated at 5 weeks after operation by gross and microscopic examination. Leakage occurred only in specimens without precultured tissue and with a collagen film. Minimal surface deformation occurred in all specimens with precultured tissue. The score on gross examination showed that transplants with precultured tissue acquired a higher score than did the others. Histological evaluation showed a minimal foreign-body response of PNIPAAm–gelatin in all specimens and higher maturity as a cartilaginous tissue in specimens with precultured tissue. These results indicate that transplantation with precultured tissue may be a suitable method for a long-term *in vivo* study.

INTRODUCTION

ORTHOPEDIC SURGEONS AND RESEARCHERS are facing the challenging problem of repairing cartilage damaged by trauma or arthritis. Although numerous tissue-engineering approaches using biomacromolecules such as collagen,[1–3] agarose,[4] alginate,[5] or synthetic polymers[6–12] have been attempted to repair damaged cartilage, a better and more reliable strategy for cartilage repair is desired.

We developed a novel system using a thermoresponsive gelatin, poly(*N*-isopropylacrylamide)-grafted gelatin (PNIPAAm–gelatin), as a moldable scaffold. A unique characteristic of PNIPAAm–gelatin, in which gelatin molecules act as a backbone and PNIPAAm as a graft chain, is its dissolution in water below 34°C and its precipitation above 34°C. PNIPAAm–gelatin solution at high concentration solidifies at physiological temperature. We applied this thermoresponsive PNIPAAm–gelatin as an *in situ*-forming moldable scaffold, which is expected to fit complex-shaped cartilaginous defects well. In our previous *in vitro* study,[13] we demonstrated that chondrocytes can survive in a three-dimensional (3D) environment of PNIPAAm–gelatin gel, express a differentiated phenotype and normal cell morphology, and secrete extracellular matrices (ECMs) spe-

[1]Department of Biomedical Engineering, Graduate School of Medicine, Kyushu University, Fukuoka, Japan.
[2]Department of Orthopaedic Surgery, Graduate School of Medicine, Kyushu University, Fukuoka, Japan.

cific to the hyaline cartilaginous tissue. Although there are still some differences in the degree of maturity between the gel and native cartilage, a prolonged period of culture of the gel resulted in a tissue-engineered cartilaginous tissue with considerably high integrity in terms of its hyaline-like appearance, the amount and component of ECMs, and mechanical properties.

However, the major potential problems of PNIPAAm–gelatin-based engineered cartilage under development are leakage of an *in situ*-formed tissue and concave deformation of the surface of the transplanted area under applied physiological stress loading. Once these occur, a transplanted site produces a deformed concave shape in the early stage of transplantation and retains this deformed shape during the following transplantation period, because the proliferative potential of chondrocytes in cartilaginous tissue is low. The leakage may be derived from redissolution of PNIPAAm–gelatin gel induced by accidental lowering of temperature during or shortly after the operation, and the deformation may derive from the immature mechanical integrity of the engineered tissue, which causes poor mechanical recovery in a physiological environment with cycles of mechanical loading and deloading. Therefore, in addition to the 3D tissue architecture mimicking a natural hyaline cartilaginous tissue, a system-engineered tissue that eliminates the shortcomings mentioned above must be developed. Our approaches under investigation include the couse of precultured tissue as the major tissue and *in situ*-formed tissue as supplementary tissue, which fills a space between the precultured tissue and adjacent native tissue, covering and sealing materials, and their combined use, as tabulated in Table 1.

Figure 1 shows the cross-sectional view of engineered cartilaginous tissues using existing materials such as collagen (Fig. 1a), *in situ*-formed PNIPAAm–gelatin gel (Fig. 1b), and the couse of PNIPAAm–gelatin gel and precultured tissue (Fig. 1c). Engineered tissues using existing materials such as collagen[1–3] and fibrin glue[14] would have a potential problem of shrinkage occurring during transplantation because of cell-driven contractility that may widen a space between the transplant and adjacent cartilage or subchondral bone (Fig. 1a). The use of a preconstructed tissue such as a collagen sponge[15] does not allow complete fitting of the shape of a chondral defect (Fig. 1a). On the other hand, PNIPAAm–gelatin as an *in situ*-gelable scaffold (Fig. 1b) or the co-use of PNIPAAm–gelatin with a precultured PNIPAAm-gelatinous tissue may enable complete fitting of a transplant to adjacent tissues (Fig. 1c).

As the second article in this series, we identify the problems mentioned above and report the short-term (5 week posttransplantation) results of PNIPAAm–gelatin-based engineered tissues in combination with covering and sealing materials applied for cartilage repair in rabbit knee joints. The emphasis was placed on the following two key issues: whether or not a 2-week precultured engineered tissue, as a more mature tissue with structural rigidity and elasticity, effectively prevents compression-induced depression in the early stage of transplantation; and whether or not a thin collagen film serves as an alternative covering material to periosteum for preventing leakage of the transplant. In this article, we report the functional adaptivity and tissue architecture of PNIPAAm–gelatin-based engineered tissues at macroscopic and microscopic levels 5 weeks after transplantation, and provide a prototype system-engineered cartilaginous tissue for further long-term evaluation.

MATERIALS AND METHODS

Isolation and expansion of chondrocytes

Chondrocytes were isolated from articular cartilage of the knee and hip joints of Japanese white rabbits (4 weeks old) by collagenase digestion (0.05% in Dulbecco's modified Eagle's medium [DMEM], 6–8 h) as previously reported.[16] The isolated chondrocytes were cultured in a 5% CO_2 atmosphere at 37°C in DMEM (Invitrogen Life Technologies, Gaithersburg, MD) with 10% fetal bovine serum (FBS; Invitrogen Life Technologies) 10 mM HEPES buffer, 44 mM $NaHCO_3$, peni-

TABLE 1. SYSTEM-ENGINEERED CARTILAGINOUS TISSUE AND THEIR COMPONENTS[a]

		Content of transplant			*Covering material*	
Group	*No. of knees*	*PNIPAAm–gelatin*	*Chondrocytes*	*Precultured tissue*	*Periosteum*	*Collagen film*
1	$n = 5$	✓	✓	—	✓	—
2	$n = 5$	✓	✓	—	—	✓
3	$n = 4$	✓	✓	✓	✓	—
4	$n = 4$	✓	✓	✓	—	✓
5a	$n = 2$	✓	—	—	✓	—
5b	$n = 2$	✓	—	—	—	✓

[a]Fibrin glue sheet was used as a sealing material for all samples.

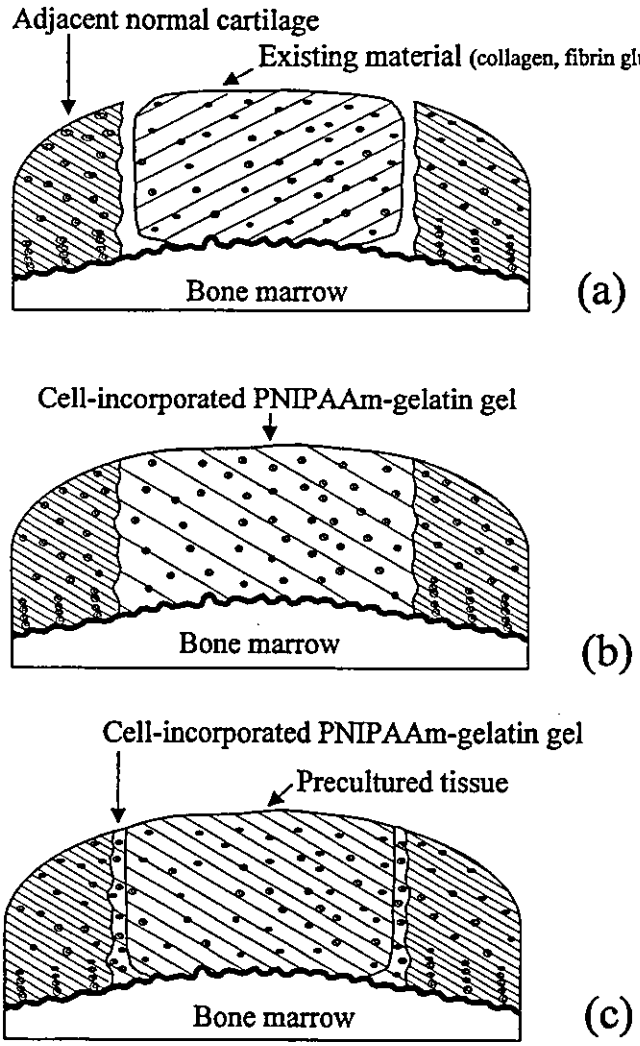

FIG. 1. Cross-sectional view of various types of engineered cartilage tissues using (a) existing materials, (b) *in situ*-formed cell-incorporated PNIPAAm–gelatin gel, and (c) both cell-incorporated PNIPAAm–gelatin gel and precultured tissue.

cillin (50 IU/mL), and streptomycin (50 μg/mL) and subcultured twice.

Preparation of poly(N-isopropylacrylamide)-grafted gelatin

The synthesis and characterization of PNIPAAm–gelatin were detailed previously.[13,17,18] Briefly, synthesis of PNIPAAm–gelatin was via the photo-iniferter quasi-living polymerization technique, which enables the production of a considerably low polydispersity index (average number of molecular weight/average weight of molecular weight) of about 1.2–1.3 (close to monodispersity). This has been verified previously.[19,20] The PNIPAAm–gelatin used in this study contained gelatin (molecular mass, 9.5×10^4 g/mol) and graft-polymerized PNIPAAm (33.5 graft chains per gelatin molecule; average molecular mass of graft chain, 1.3×10^5 g/mol). Sterilization of PNIPAAm–gelatin was performed by filtering the aqueous solution of PNIPAAm–gelatin with a sterilizing filter (bottle top filter; Corning Life Sciences, New York, NY) and then freeze-drying.

Preparation of tissue-engineered cartilage in vitro

Precultured tissues (i.e., cartilage tissues engineered *in vitro*) for transplantation were prepared as follows. DMEM solution containing three-time-passaged chondrocytes in monolayer culture (3.0×10^7 cells/mL) was mixed with an equal volume of 10% PNIPAAm–gelatin–DMEM solution at room temperature to give a final concentration of 1.5×10^7 cells/mL (concentration of PNIPAAm–gelatin, 5 w/v%). Twenty microliters of mixed solution was poured into each well of a 12-well culture cluster (Corning Life Sciences) and incubated for 10 min at 37°C. After gelatin, DMEM supplemented with

10% FBS and L-ascorbic acid (50 μg/mL) was added to each well. The culture was performed in a 5% CO_2 atmosphere at 37°C for 2 weeks. The medium was changed twice a week.

Surgical procedure for chondrocyte transplantation

Twenty-four knees of 12 mature Japanese white rabbits (weight, 3.8–4.0 kg) were used for this study. The animals were anesthetized by intravenous injection of ketamine at 100 mg/kg of body weight and xylazine at 30 mg/kg of body weight. The knees were shaved, disinfected, and approached by medial parapatellar incision. The patella was then dislocated laterally, and a full-thickness chondral defect in the patellar cartilage (3.5 mm in diameter; depth, ~0.5 mm) was made with a stainless steel biopsy punch and scalpel. A hole through the subchondral bone plate to the bone marrow was produced with an 18-gauge needle in the area of the chondral defect.

Five different transplantation methods were performed (Table 1). Figure 2 illustrates the surgical procedures. For group 1 (Fig. 1b, $n = 5$), a free periosteal flap harvested from the medial proximal tibia was sutured (with the cambium layer facing the defect) to the adjacent cartilage rim of the defect by six interrupted sutures with 9-0 nylon (Ethilone; Johnson & Johnson, Raynham, MA). Five points of the periosteal flap were sutured, and the last one was sutured after injection with a phosphate-buffered saline (PBS) solution of cells and PNIPAAm–gelatin (cell density, 1.5×10^7 cells/mL; concentration of PNIPAAm–gelatin, 5 w/v%). Moreover, the suture line was covered with a fibrin glue sheet (TachoComb; Torii Pharmaceutical, Tokyo, Japan) to prevent solution leakage. For group 2 (Fig. 1b, $n = 5$), the defect was first covered with a thin collagen film (thickness, ~70 μm; Nippi, Tokyo, Japan) accreted with fibrin glue sheet of the same diameter, using the same method as described above. Next, the PBS solution of cells and PNIPAAm–gelatin was poured into the defect, and allowed to gel. Finally, covering with the fibrin glue sheet to seal the suture line was performed after the last point of the cover was sutured. For group 3 (Fig. 1c, $n = 4$), the defect was covered with the periosteal flap by suturing. After the aforementioned precultured tissue (thickness, ~500 μm; rim was shaped to fit the diameter of the defect) was transplanted into the defect, the

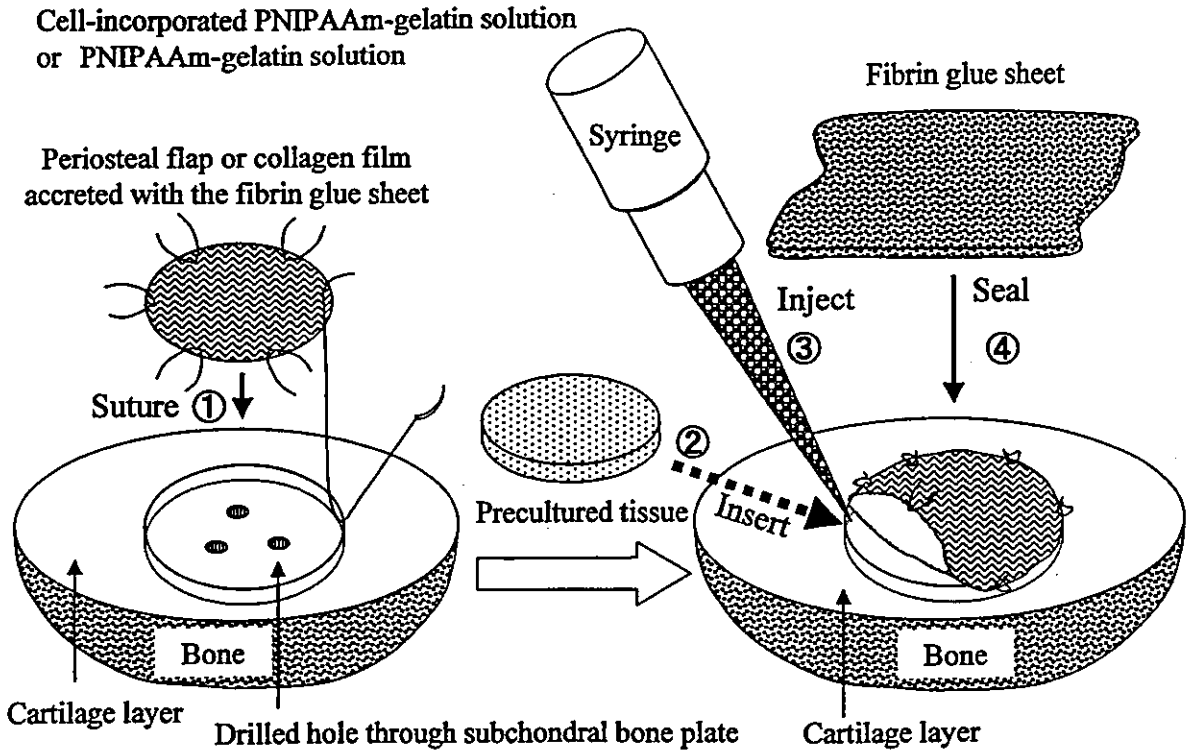

FIG. 2. Schematics of the surgical procedure. A full-thickness chondral defect (3.5 mm in diameter) down to a calcified zone was generated and subsequent drilling through subchondral bone was performed in the rabbit patella. Then, (1) the covering material was sutured at 5 points with 9-0 nylon, and (2, 3) the transplant precultured tissue and/or cell-incorporated PNIPAAm–gelatin) was placed over the defect. After gelation, the last suture was performed. Finally, (4) the transplanted area was sealed with a fibrin glue sheet.

PBS solution of cells and PNIPAAm–gelatin was poured into the space between the transplant and adjacent normal tissues. Last, the fibrin glue sheet for sealing the suture line was used to cover the transplanted area after the last suture. For group 4 (Fig. 1c, $n = 4$), the covering material was thin collagen film accreted with fibrin glue sheet. The PBS solution of cells and PNIPAAm–gelatin and precultured tissue were transplanted, using the same method as for group 3. Covering with a fibrin glue sheet to seal the suture line was performed. For group 5a (Fig. 1b, $n = 2$), which was a control group, the defect was covered with the periosteal flap and the fibrin glue sheet; the content of the transplant was PNIPAAm–gelatin solution without cells. For group Sb (Fig. 1b, $n = 2$), which was also a control group, the defect was covered with thin collagen film and fibrin glue sheet; the content of the transplant was PNIPAAm–gelatin solution without cells. Thin collagen film accreted with fibrin glue sheet served as a covering material and only PNIPAAm–gelatin solution was used for transplantation. The wounds of the knee joints were closed, and the animals were allowed to walk freely in their cages, housed at room temperature after the operation.

Macroscopic evaluation

All animals were killed by injection of ketamine at 5 weeks postoperatively. The surfaces of the transplanted area and adjacent cartilage were observed carefully and scored, using the scoring scale adapted from previously reported methods,[21,22] for integrity of the transplant to the adjacent cartilage, smoothness of the surface of the transplanted areas, and degree of filling of the transplant. A more detailed description is given in the footnote to Table 2. Scores for each category are summed to a total maximum score of 6.

Histological and immunohistochemical staining

The patellas were dissected and fixed in 50% methanol and 50% formaldehyde for 24 h, defatted, decalcified with 10% formic acid, and embedded in paraffin. Serial sections (5 μm thick) were sliced from the embedded tissue specimens perpendicular to the articular surface and mounted onto glass slides. Serial sections were stained with hematoxylin and eosin (H&E) and safranin O/fast green for sulfated glycosaminoglycan (s-GAG) by the standard histochemical technique. For immunohistochemical detection of type II collagen, using a previously reported method,[23] a monoclonal mouse antibody against type II collagen [anti-hCL(II); Daiichi Fine Chemicals, Toyama, Japan] was used. Briefly, the sections deparaffinized were first treated with 0.1% trypsin for 30 min. The sections were subsequently treated with testicular hyaluronidase (type I-S, 1.45 IU/mL; Sigma, St. Louis, MO) and treated last with chondroitinase ABC (0.25 IU/mL; Sigma) at 37°C for 30 min before overnight incubation at room temperature with primary antibodies. The primary antibody was diluted with PBS containing 0.1% Triton X-100 (Sigma) and 0.7% carrageenan (Sigma). The antibody against type II collagen was used at 1:1000 dilution (protein concentration, 500 ng/mL). The sections were incubated with a biotinylated rabbit anti-mouse IgG antibody (Nichirei, Tokyo, Japan) at room temperature for 60 min and subsequently incubated in 150 mL of methanol with 1.5 mL of H_2O_2 at room temperature for 30 min. After washing with PBS, the sections were incubated with streptavidin-conjugated immunoperoxidase (Nichirei). The signal was finally visualized as a brown reaction product from the peroxidase substrate 3,3′-diaminobenzidine (DAB; Merck, Darmstadt, Germany).

Statistical analysis

Statistical analysis was performed with the StatView 5.0 program (SAS Institute, Cary, NC). Data were shown as means ± standard deviation (SD). The values were subjected to statistical analysis using the Kruskal–Wallis test.

RESULTS

Figure 2 illustrates the surgical procedure used. After a full-thickness chondral defect (3.5 mm in diameter and ~0.5 mm in depth) was mechanically generated and a hole through the subchondral bone plate was subsequently made, the covering material, a periosteum or a thin collagen film, was sutured to the adjacent cartilage rim at five points. The mixture of chondrocytes and PNIPAAm–gelatin was then injected. The mixture (5–10 μL) was poured into the defect, and allowed to gel under physiological temperature (groups 1 and 2 in Table 1). The last suture (the sixth) was then performed. Last, the suture line was sealed with a fibrin glue sheet. On the other hand, precultured PNIPAAm–gelatin gel in which chondrocytes were cultured for 2 weeks was plated at the bottom of the defect after suturing a covering material, using the method described above (groups 3 and 4 in Table 1). The space between the precultured tissue and adjacent native tissue was then filled with the mixture of cells and PNIPAAm–gelatin. The covering, sealing, and suturing methods were the same as those mentioned above. All samples were harvested 5 weeks after surgery. One rabbit died because of anesthesia overdose. Thus, 22 knees were evaluated in this study. The scoring of the maturity of the transplant by gross evaluation according to categories such as integrity, smoothness of surface, and degree of filling is tabulated in Table 2. A score of 2.0 indicates the best performance and a score of 0.0 the poorest performance in each category. The degree of maturity of transplanted tissues as evaluated by microscopic

TABLE 2. MACROSCOPIC MORPHOLOGICAL EVALUATION OF TRANSPLANTED AREA[a]

Group	*No. of knees*	*Integrity*	*Smoothness*	*Degree of filling*	*Total (maximum, 6)*
1	$n = 5$	2.0 ± 0.0	0.0 ± 0.0	1.0 ± 0.0	3.0 ± 0.0
2	$n = 5$[b]	1.2 ± 1.1	0.2 ± 0.55	0.6 ± 0.55	2.0 ± 1.87
3	$n = 4$	2.0 ± 0.0	0.25 ± 0.5	2.0 ± 0.0	4.25 ± 0.5
4	$n = 4$	2.0 ± 0.0	0.5 ± 0.6	2.0 ± 0.0	4.5 ± 0.58
5a	$n = 2$	2.0 ± 0.0	0.0 ± 0.0	0.5 ± 0.7	2.5 ± 0.7
5b	$n = 2$	2.0 ± 0.0	0.0 ± 0.0	0.0 ± 0.0	2.0 ± 0.0

[a]Macroscopic evaluation using scoring scale adapted from Bruns *et al.*[21] and Moran *et al.*[22]: integration to adjacent native cartilage—full, 2; partial, 1; none, 0; smoothness of cartilage surface—smooth, 2; intermediate, 1; rough, 0; cartilage surface, degree of filling—flush, 2; slight depression, 1; depression or overgrowth, 0.

evaluation was determined on the basis of cell morphology, and contents of s-GAG and type II collagen.

Macroscopic findings

Leakage occurred in two of the five knees in group 2. No leakage occurred in the other groups. Gross observation of nonleaking tissues revealed that irrespective of groups, transplanted areas, which were connected to the adjacent cartilage, remained partially or fully covered with a fibrous membrane (Fig. 3). Therefore, in all samples except leaking samples, the score of integrity of the transplanted area connected to the adjacent cartilage was 2.0 (maximum, 2.0; Table 2). In the group using periosteum as a covering material, almost all surfaces were rough. The scores of surface smoothness in groups 1 and 3 were 0.0 ± 0.0 and 0.25 ± 0.5, respectively (Table 2). In the groups using a collagen film as a covering material (groups 2, 4, and 5b), collagen films were partially biodegraded in some samples (Fig. 3a, c, and e). In these groups, some surfaces of the neocartilage were relatively smooth beneath the covering material. The scores of surface smoothness in groups 2 and 4 were 0.2 ± 0.55 and 0.5 ± 0.6, respectively (Table 2). As for the degree of filling, no depression of the surface occurred in groups 3 and 4 (both scores were 2.0 ± 0.0; Table 2). On the other hand, all the surfaces in groups 1, 2, and 5 were depressed to some extent. The scores of the degree of filling in groups 1, 2, 5a, and 5b were 1.0 ± 0.0, 0.6 ± 0.55, 0.5 ± 0.7, and 0.0 ± 0.0, respectively (Table 2). The total score in Table 2 showed that there is no significant difference among the groups. The total scores of the groups with the precultured tissue (groups 3 and 4) were relatively higher than those of groups 2, 5a, and 5b.

Histological evaluation

H&E-stained sections of all groups (Fig. 4a–d) showed that no inflammatory cell or vascularization was detected in the transplanted PNIPAAm–gelatin gel. Inflammatory cells (mainly lymphocytes and fibroblast-like cells) were seen in a bone marrow area that was damaged during the operation. Moreover, neither necrosis nor encapsulated areas around the transplanted tissues were seen in any of the sections of all the groups. As for cell morphology, round-shaped cells were predominant in groups 3 and 4. On the other hand, the ratios of the population of elongated cells to the total number of cells in groups 1 and 2 were higher than those in groups 3 and 4. In the groups in which periosteum was used as the covering material (groups 1, 3, and 5a), periosteum was not degraded. Most of the surfaces of these groups tended to be rough (Fig. 4a and c). Figure 4a shows that periosteum overgrew, resulting in a wavy surface appearance. On the other hand, in the groups in which a collagen film was used as the covering material (groups 2, 4, and 5b), the collagen film was partially degraded in most sections (Fig. 4b and d). In the groups in which precultured tissue (groups 3 and 4) was embedded, column formation of the cells was observed in some of the samples (Fig. 4a and b).

Safranin O-stained tissue sections of all the groups except the control groups demonstrated a distribution of s-GAG, a product of differentiated cells, throughout the transplanted tissue (Fig. 4e–h). The stained part of the tissue, however, was not homogeneous. Local accumulation of s-GAG was often observed in some samples, irrespective of group. The staining intensity of safranin O in the transplanted tissue was lower than that of the adjacent native cartilaginous tissue in almost all the samples of all the groups. There were no considerable differences in the staining intensity between the groups, although parts stained with high intensity were noted in each group.

The sections immunostained for type II collagen demonstrated that type II collagen was secreted by redifferentiated chondrocytes throughout the transplant. Most of the tissue was homogeneously stained but local high intensity-stained parts were often observed in all groups (Fig. 4i–l). Generally, the intensity of type II collagen in the transplanted tissue was lower than that in the adjacent native cartilaginous tissue in almost all the samples of all the groups, indicating that the accumulation of type II collagen in the regenerative tissue

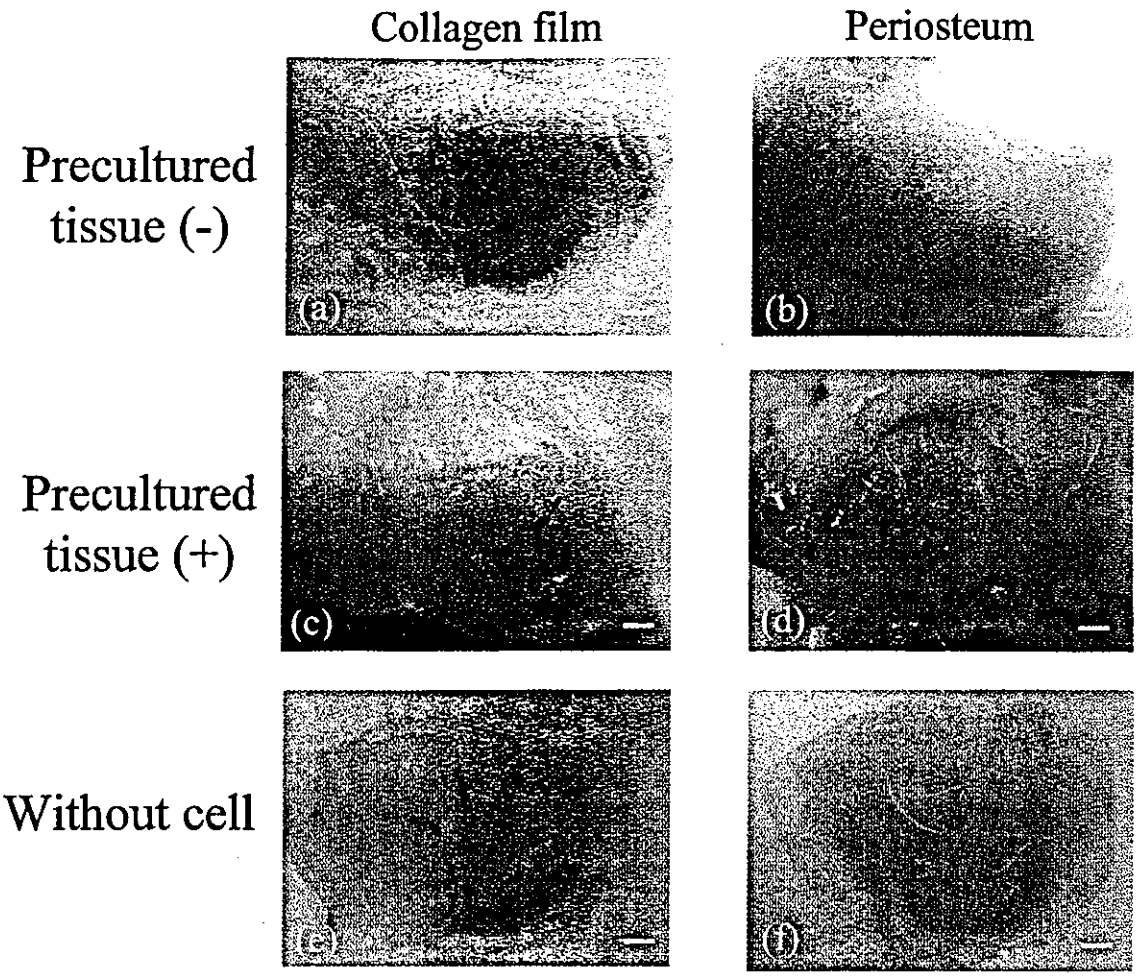

FIG. 3. Photographs of surfaces of transplanted area in harvested patellae. (**a**, **c**, and **e**) Group using a thin collagen film as a covering material. (**b**, **d**, and **f**) Group using a periosteal flap as a covering material. *Top row*: Group transplanted with cell-incorporated PNIPAAm–gelatin. *Middle row*: Group transplanted with the co-use of cell-incorporated PNIPAAm–gelatin gel and precultured tissue. *Bottom row*: Group transplanted with only PNIPAAm–gelatin gel. Scale bars: 1 mm.

was still less than that in the normal tissue 5 weeks after transplantation.

DISCUSSION

To reconstruct cartilaginous tissue, chondrocytes or mesenchymal stem cells have been embedded in various preformed scaffolds such as microporous collagen sponge[15] and gelatin sponge[24] or inoculated in *in situ*-formable scaffolds such as fibrin glue,[14] and then transplanted with or without preculture *in vitro*. These systems, when clinically applied, may have both advantages and disadvantages, which are inherent to the system. In our strategic approach using PNIPAAm–gelatin as a moldable scaffold and matrix, leakage of the transplanted gel and concave deformation of the surface of the transplanted area were two major problems considered. In fact, transplants of *in situ*-formed engineered tissue covered with only a fibrin glue sheet had a high leakage rate (seven of nine transplants leaked, approximately 78%). This is probably due to the redissolution of the PNIPAAm–gelatin gel at a temperature below 34°C during or shortly after the operation, and the ineffectiveness of the fibrin glue sheet in preventing leakage of the transplant. To solve the two major problems, we attempted the use of precultured tissue and a suturing technique that uses covering materials to prevent surface deformation and leakage of the transplant, respectively. Our previous study showed that engineered tissue cultured for 2 weeks has higher compression strength and better recovery of the original shape after mechanical loading than freshly prepared engineered tissue.[13] These results support the potential use of precultured tissues for preventing surface deformation.

In this study, we focused on which type of covering

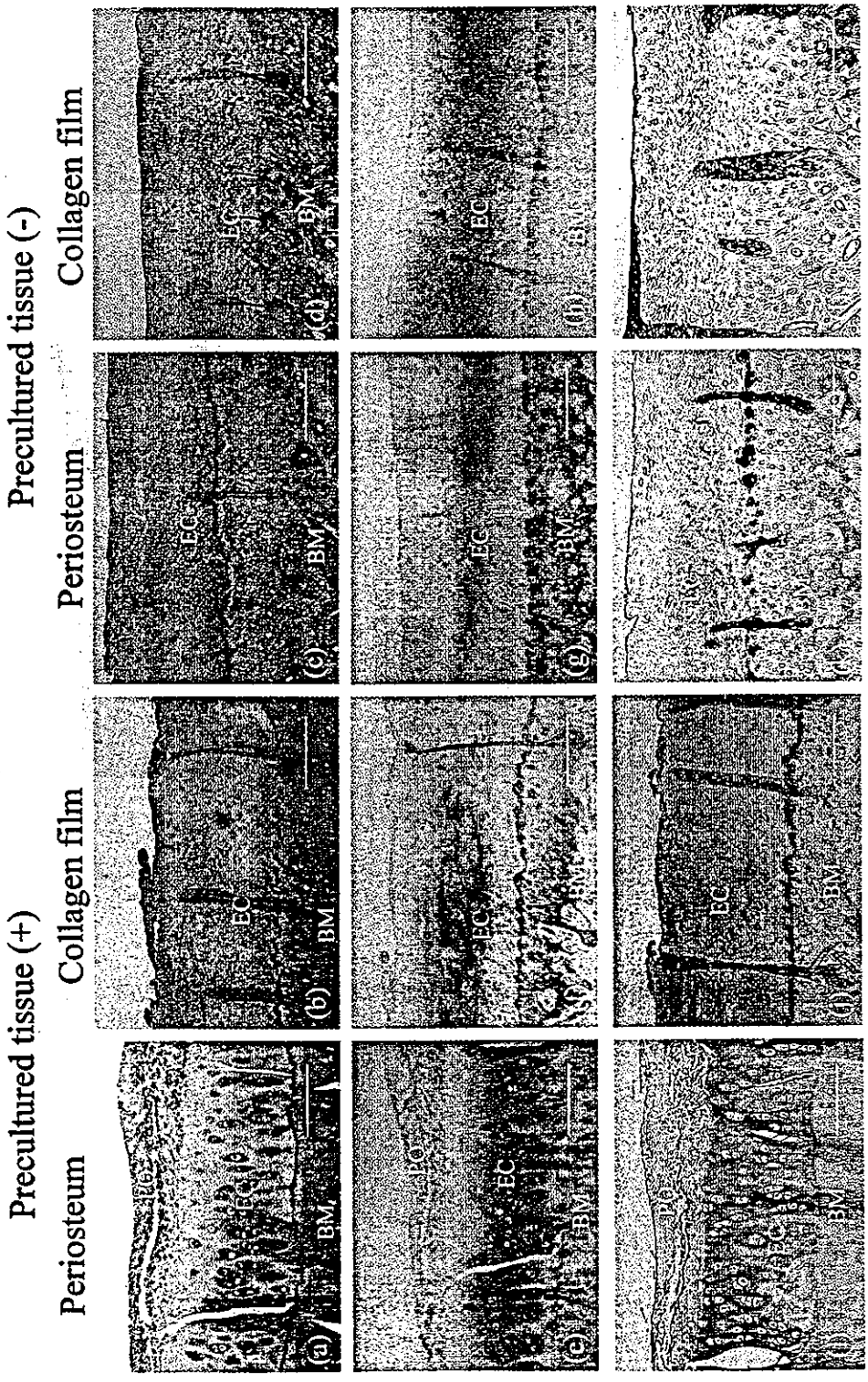

FIG. 4. Histological cross-sections of the transplants 5 weeks postoperatively. They are stained with (a–d) H&E, (e–h) safranin O/fast green, and (i–l) type II collagen antibody. Original magnification: (a–l) ×100. Scale bars: 200 μm. PO, periosteum; EC, engineered cartilage; BM, bone marrow.

material, periosteum or collagen film, is most suitable for preventing leakage of the engineered tissue as well as tissue deformation, whether *in vitro*-precultured tissue reduces or eliminates the deformation problem, and which engineered tissue is sufficiently remodeled for constructing normal cartilaginous tissue architecture or morphology 5 weeks after transplantation.

As shown in Table 1, for *in situ*-gelled tissues, no leakage of the tissues occurred when using periosteum as the covering material and approximately 40% leakage occurred when using collagen film (group I versus group 2). On the other hand, for the couse of precultured tissues and *in situ*-gelled tissues, regardless of the type of covering material, no leakage was observed (groups 3 and 4). Thus, suturing of the periosteal flap as a covering material to the adjacent cartilage rim and the use of precultured tissues were apparently effective for preventing leakage. Because collagen film tends to be torn by mechanical stretching, especially at the suturing points, the leakages occurring in the early period of transplantation may be due to breaking of the collagen film. In limited experiments performed by the authors, it is suggested that periosteum is a better covering material than collagen film.

Histological evaluation of transplants harvested from all groups (H&E staining; Fig. 4a–d) showed that no inflammatory cells were present in the PNIPAAm–gelatin gel and no encapsulated tissue formation around the gel occurred, indicating that foreign-body response induced by PNIPAAm–gelatin was minimal (groups 1–5). The cells in the transplanted tissues were round or elongated and trapped in lacunae similar to native hyaline cartilage (groups 1–4). The presence of elongated cells suggests premature redifferentiation to normal chondrocytes or partial dedifferentiation of the articular chondrocytes to fibrochondrocytes. Column formation of transplanted cells in the groups with precultured tissue indicated that the cells grew in an appropriate mechanical stress environment (groups 3 and 4). As for integration with the adjacent cartilage, almost all the transplants (groups 1–5) except the leaked samples were continuous with adjacent cartilage macroscopically (Fig. 3) and microscopically (Fig. 4). Although integration of the transplanted tissue with subchondral bone was also realized in almost all the samples of all the groups, some fissures were observed in the sections (Fig. 4). These fissures were probably produced artificially, because the fissures were perfectly empty, indicating the absence of both cells and tissues. Gross evaluation showed that almost all surfaces of the transplanted area in all groups were rough (groups 1–5) and the collagen film was partially biodegraded in some samples of groups 2, 4, and 5b (Fig. 3a and e).

Microscopic examination of samples from groups 2 and 4 revealed that some surfaces beneath degraded collagen film were smooth (Fig. 4d, h, and l). A comparatively smooth surface of the thin collagen film may contribute to the smooth surfaces of the samples in the group using collagen film. On the other hand, overgrown periosteum was microscopically observed in some samples of the group using periosteum (groups 1 and 3), which exhibited a wavy surface along the transplanted area (Fig. 4a, e, and i). This phenomenon probably occurred because the periosteum was autogenous tissue. In clinical reports, the periosteal flap as the covering material overgrew at a comparatively high rate.[25,26] The advantages of thin collagen film as an alternative to periosteum are biodegradability, which contribute to the nonhypertrophic surface, and easy availability. In addition, the disadvantage thin collagen film is difficulty in handling due to the fragile nature of collagen film. With regard to the surface deformation of the transplanted area, deformation occurred as expected in the groups without precultured tissue (groups 1, 2, and 5). On the other hand, all surfaces of the transplanted area in groups 3 and 4 exhibited a flush surface with the adjacent cartilage. These results indicate that prevention of surface deformation of the transplanted area using precultured tissue was effective. Although macroscopic scoring showed that there was no significant difference among the groups, the deformed surface of the transplanted area in all the samples from groups 1 and 2 was a critical problem. Thus, the method of transplantation in groups 1 and 2 was not suitable for appropriate cartilage repair. Histological evaluation of all groups showed that ECMs in the transplant were secreted, but that the amount of ECMs was not sufficient to construct well-formed hyaline cartilaginous tissue throughout the tissue.

These results suggest that the couse of cell-incorporated PNIPAAm–gelatin *in situ*-formed gel and precultured tissue irrespective of the covering material (groups 3 and 4) provides a suitable method for reconstructing cartilaginous tissues with good integrity of the transplant to the adjacent tissues, smooth surface, minimal surface deformation, and no leakage of the transplant. A long-term transplantation study for groups 3 and 4 is now underway to develop a system-engineered cartilaginous tissue that will be utilized for clinical trials.

ACKNOWLEDGMENT

This study was financially supported by a Grant-in-Aid for Scientific Research (A2-12358017 and B2-12470277) from the Ministry of Education, Culture, Sports, Science, and Technology of Japan.

REFERENCES

1. Wakitani, S., Goto, T., Young, R.G., Mansour, J.M., Goldberg, V.M., and Caplan, A.I. Repair of large full-thickness

articular cartilage defects with allograft articular chondrocytes embedded in a collagen gel. Tissue Eng. **4,** 429, 1998.
2. Katsube, K., Ochi, M., Uchio, Y., Maniwa, S., Matsusaki, M., Tobita, M., and Iwasa, J. Repair of articular cartilage defects with cultured chondrocytes in Atelocollagen gel: Comparison with cultured chondrocytes in suspension. Arch. Orthop. Trauma Surg. **120,** 121, 2000.
3. Nehrer, S., Breinan, H.A., Ramappa, A., Hsu, H.P., Minas, T., Shortkroff, S., Sledge, C.B., Yannas, I.V., and Spector, M. Chondrocyte-seeded collagen matrices implanted in a chondral defect in a canine model. Biomaterials **19,** 2313, 1998.
4. Rahfoth, B., Weisser, J., Sternkopf, F., Aigner, T., von der Mark, K., and Brauer, R. Transplantation of allograft chondrocytes embedded in agarose gel into cartilage defects of rabbits. Osteoarthritis Cartilage **6,** 50, 1998.
5. Guo, J.F., Jourdian, G.W., and MacCallum, D.K. Culture and growth characteristics of chondrocytes encapsulated in alginate beads. Connect. Tissue Res. **19,** 277, 1989.
6. Messner, K., and Gillquist, J. Synthetic implants for the repair of osteochondral defects of the medial femoral condyle: A biomechanical and histological evaluation in the rabbit knee. Biomaterials **14,** 513, 1993.
7. Freed, L.E., Vunjak-Novakovic, G., Biron, R.J., Eagles, D.B., Lesnoy, D.C., Barlow, S.K., and Langer, R. Biodegradable polymer scaffolds for tissue engineering. Biotechnology **12,** 689, 1994.
8. Freed, L.E., Marquis, J.C., Nohria, A., Emmanual, J., Mikos, A.G., and Langer, R. Neocartilage formation in vitro and in vivo using cells cultured on synthetic biodegradable polymers. J. Biomed. Mater. Res. **27,** 11, 1993.
9. Elisseeff, J., Anseth, K., Sims, D., McIntosh, W., Randolph, M., Yaremchuk, M., and Langer, R. Transdermal photopolymerization of poly(ethylene oxide)-based injectable hydrogels for tissue-engineered cartilage. Plast. Reconstr. Surg. **104,** 1014, 1999.
10. Elisseeff, J., McIntosh, W., Anseth, K., Riley, S., Ragan, P., and Langer, R. Photoencapsulation of chondrocytes in poly(ethylene oxide)-based semi-interpenetrating networks. J. Biomed. Mater. Res. **51,** 164, 2000.
11. Ameer, G.A., Mahmood, T.A., and Langer, R. A biodegradable composite scaffold for cell transplantation. J. Orthop. Res. **20,** 16, 2002.
12. Wyre, R.M., and Downes, S. An in vitro investigation of the PEMA/THFMA polymer system as a biomaterial for cartilage repair. Biomaterials **21,** 335, 2000.
13. Ibusuki, S., Fujii, Y, Iwamoto, Y, and Matsuda, T. Tissue-engineered cartilage using an injectable and *in situ* gelable thermoresponsive gelatin: Fabrication and *in vitro* performances. Tissue Eng. **9,** 301, 2003.
14. Homminga, G.N., Buma, P., Koot, H.W., van der Kraan, P.M., and van den Berg, W.B. Chondrocyte behavior in fibrin glue in vitro. Acta Orthop. Scand. **64,** 441, 1993.
15. Sellers, R.S., Zhang, R., Glasson, S.S., Kim, H.D., Peluso, D., D'Augusta, D.A., Beckwith, K., and Morris, E.A. Repair of articular cartilage defects one year after treatment with recombinant human bone morphogenetic protein-2 (rhBMP-2). J. Bone Joint Surg. Am. **82,** 151, 2000.
16. Yasui, N., Osawa, S., Ochi, T., Nakashima, H., and Ono, K. Primary culture of chondrocytes embedded in collagen gels. Exp. Cell Biol. **50,** 92, 1982.
17. Ohya, S., Nakayama, Y., and Matsuda, T. Material design for artificial extracellular matrix: Cell entrapment in poly(*N*-isopropylacrylamide) (PNIPAM) grafted gelatin hydrogel. J. Artif. Organs **4,** 308, 2001.
18. Morikawa, N., and Matsuda, T. Thermoresponsive artificial extracellular matrix: *N*-Isopropylacrylamide-graft-copolymerized gelatin. J. Biomater. Sci. Polym. Ed. **13,** 167, 2002.
19. Nakayama, Y., and Matsuda, T. In situ observation of dithiocarbamate-based surface photograft copolymazation using quartz crystal microbalance. Macromolecules **32,** 5405, 1999
20. Nakayama, Y., Miyamura, M., Hirano, Y., Goto, K., and Matsuda, T. Preparation of poly(ethylene glycol)-polystyrene block copolymers using photochemistry of dithiocarbamate as a reduced cell-adhesive coating material. Biomaterials **20,** 963, 1999
21. Bruns, J., Kersten, P., Lierse, W., and Silbermann, M. Autologous rib perichondrial grafts in experimentally induced osteochondral lesions in the sheep-knee joint: morphological results. Virchows Arch. A Pathol. Anat. Histopathol. **421,** 1, 1992
22. Moran, M.E., Kim, H.K., and Salter, R.B. Biological resurfacing of full-thickness defects in patellar articular cartilage of the rabbit: Investigation of autogenous periosteal grafts subjected to continuous passive motion. J. Bone Joint Surg. Br. **74,** 659, 1992
23. Kumagai, J., Sarkar, K., Uhthoff, H.K., Okawara, Y., and Ooshima, A. Immunohistochemical distribution of type I, II and III collagens in the rabbit supraspinatus tendon insertion. J. Anat. **185,** 279, 1994.
24. Ponticiello, M.S., Schinagl, R.M., Kadiyala, S., and Barry, F.P. Gelatin-based resorbable sponge as a carrier matrix for human mesenchymal stem cells in cartilage regeneration therapy. J. Biomed. Mater. Res. **52,** 246, 2000.
25. Brittberg, M., Lindahl, A., Nilsson, A., Ohlsson, C., Isaksson, O., and Peterson, L. Treatment of deep cartilage defects in the knee with autologous chondrocyte transplantation. N. Engl. J. Med. **331,** 889, 1994.
26. Peterson, L., Minas, T., Brittberg, M., Nilsson, A., Sjogren-Jansson, E., and Lindahl, A. Two- to 9-year outcome after autologous chondrocyte transplantation of the knee. Clin. Orthop. **374,** 212, 2000.

Address reprint requests to:
Takehisa Matsuda, Ph.D.
Department of Biomedical Engineering
Graduate School of Medicine
Kyushu University
3-1-1 Maidashi, Higashi-ku
Fukuoka 812-8582, Japan

E-mail: matsuda@med.kyushu-u.ac.jp

ELSEVIER

Journal of Orthopaedic Research 22 (2004) 104–109

Journal of Orthopaedic Research

www.elsevier.com/locate/orthres

Anatomical analysis of the femoral condyle in normal and osteoarthritic knees

Shuichi Matsuda [a,*], Hiromasa Miura [a], Ryuji Nagamine [a], Taro Mawatari [a], Masami Tokunaga [b], Ryotaro Nabeyama [a], Yukihide Iwamoto [a]

[a] *Department of Orthopaedic Surgery, Graduate School of Medical Sciences, Kyushu University, 3-1-1 Maidashi, Higashi-Ku, Fukuoka City, Fukuoka 812-8582, Japan*

[b] *Fukuoka Orthopaedic Hospital, 2-10-50 Yanagouchi, Minami-Ku, Fukuoka city, Fukuoka 815-0063, Japan*

Accepted 21 May 2003

Abstract

It is important to understand anatomical feature of the distal femoral condyle for treatment of osteoarthritic knees. Detailed measurement of the femoral condyle geometry, however, has not been available in osteoarthritic knees including valgus deformity. This study evaluated femoral condyle geometry in 30 normal knees, 30 osteoarthritic knees with varus deformity, and 30 osteoarthritic knees with valgus deformity using radiographs and magnetic resonance imaging (MRI). In radiographic analysis in the coronal plane, the femoral joint angle (lateral angle between the femoral anatomic axis and a tangent to femoral condyles) was 83.3° in the normal knees, 83.8° in the varus knees, and 80.7° in the valgus knees. In MRI analysis in the axial plane, the posterior condylar tangent showed 6.4° of internal rotation relative to the transepicondylar axis in the normal knees, 6.1° in the varus knees, and 11.5° in the valgus knees. These results suggested that there was no hypoplasia of the medial condyle in the varus knees, but the lateral condyle in the valgus knees was severely distorted. Surgeons should take this deformity of the lateral femoral condyle into account when total knee arthroplasty is performed for a valgus knee.

Keywords: Knee; Osteoarthritis; Surface geometry; Magnetic resonance imaging

Introduction

Correct rotational alignment of the femoral component is essential for achieving proper varus and valgus stability and patellar tracking in total knee arthroplasty. Anatomical and biomechanical studies have shown that the transepicondylar axis is a reliable rotational landmark [7,10–12,23]. The anteroposterior (AP) axis, which is approximately perpendicular to the epicondylar axis, is used as a rotational landmark for the femoral component [3]. On the other hand, posterior condyles are also used as a rotational landmark when total knee arthroplasty is performed, because the posterior condyles can be more easily identified intraoperatively than the transepicondylar axis.

Current cutting guides for the distal femur allow externally rotation of the femoral component a few degrees relative to the posterior condyles. However, the anatomical features of the posterior condyles vary with deformity, and the use of the fixed externally rotated angle for all knees can result in rotational malalignment of the femoral component. Varus knees do not demonstrate hypoplasia or severe wear of the posterior part of the medial condyle [13], but the lateral femoral condyle may appear hypoplastic in valgus knees [16,20]. Detailed geometric measurements of the distal femur, however, have not been available in osteoarthritic knees with valgus deformity. This study evaluated the surface geometry in normal, varus, and valgus knees using magnetic resonance (MRI) imaging and radiographs to determine whether hypoplasia of the lateral condyle exists in the valgus knee.

Methods

The subjects gave informed consent and an institutional review board approved the study. Thirty normal knees in 27 healthy volunteers, 30 osteoarthritic knees with varus deformity in 30 patients and

* Corresponding author. Tel.: +81-92-642-5447; fax: +81-92-642-5507.

E-mail address: mazda@ortho.med.kyushu-u.ac.jp (S. Matsuda).

0736-0266/$ - see front matter © 2003 Orthopaedic Research Society. Published by Elsevier Ltd. All rights reserved.
doi:10.1016/S0736-0266(03)00134-7

Table 1
Clinical data for each group

Parameter	Normal knees	Varus knees	Valgus knees
Age	66.2 ± 6.5	67.9 ± 5.0	71.5 ± 11.3
Gender			
Male	10	8	2
Female	20	22	28
Knee society score	100.0 ± 0.0	49.3 ± 16.9	54.4 ± 18.8

30 osteoarthritic knees with valgus deformity in 26 patients were evaluated using MRI (Table 1). Subjects with the normal knees had no knee symptoms, and no osteoarthritic changes were detected on plain radiographs. Physical examination showed no abnormal findings. Patients with the varus and valgus knees had signs and symptoms of osteoarthritis. Standing radiographs showed the complete loss of the medial joint space in the varus knees, and of the lateral joint space in the valgus knees. Based on the case history, physical examination, and laboratory tests, patients with rheumatoid arthritis and other inflammatory diseases or metabolic conditions were excluded from the study. No subject had a history of injury to the knees.

MRI analysis

MRI was performed using a 0.5 T whole body MR imaging system (MRP-5000AD, Hitachi Medical Corp, Kashima, Japan) with an extremity coil, and all the subjects were restrained from moving during the scanning process. Pulse sequences were T1-weighted images (500/20, TR/TE). The direction of axial slice imaging placed the slice perpendicular to the femoral mechanical axis in the coronal plane and perpendicular to the long axis of the femur in the sagittal plane. The axial slice on the most prominent part of both femoral condyles was selected for analysis.

The transepicondylar axis was defined as a line between the most medial and the most lateral prominences of the epicondyles, and the posterior condylar tangent as a line connecting the posterior aspects of the femoral condyles [3,13] (Fig. 1). Articular boundaries of the femoral condyles were used for posterior condylar tangent. The AP axis was a line connecting the deepest part of the patellar groove anteriorly and the mid point between the most posterior part of the condyle [3]

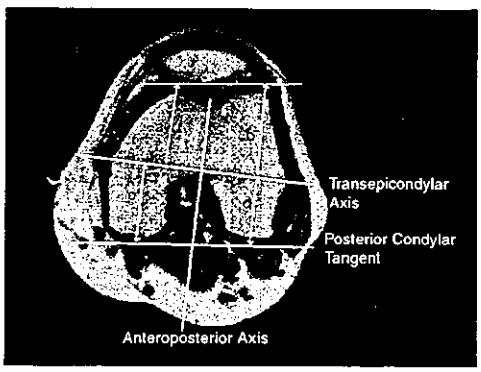

Fig. 1. Magnetic resonance image of the axial view of the distal femur. A line was drawn perpendicular to the transepicondylar axis from the most anterior part of each anteorior condyle. The distance (a) was defined as AP dimension of the anterior part of the medial femoral condyle and the distance (b) was defined as that of the lateral femoral condyle. A line was drawn perpendicular to the transepicondylar axis from the most posterior part of each posterior condyle. The distance (c) was defined as the AP dimension of the posterior part of the medial femoral condyle and the distance (d) was defined that of the lateral femoral condyle.

Fig. 2. Magnetic resonance image of the sagittal view of the distal femur. A line (Line A–B) was drawn from the most distal point on the surface articulating with the tibia (A) to the most superior point of the femoral articular surface of the posterior condyle (B). Another line was drawn perpendicular to Line A–B from its midpoint to the femoral articular surface. The point where this line met the femoral articular surface was defined as point C. The arc A–B was defined as the posterior part of the femoral condyle, and point A, B, and C were used for calculation of the radius in the posterior part of the condyle.

(Fig. 1). The angle between the transepicondylar axis and the posterior condylar tangent and the angle between the line perpendicular to the AP axis and the posterior condylar tangent were measured and compared among the normal, varus and valgus knees. The lateral angle between the transepicondylar axis and the AP axis was also measured in each group. The AP dimensions of both the medial and lateral condyles were measured (Fig. 1).

Sagittal plane sections through the most prominent part of both femoral condyles were used for measurement. The articular surface of each condyle was divided into distal and posterior parts (Fig. 2). The posterior part was assumed to fit a circular arc [7,13], and the radius of the arc was calculated using three points on the articular surface of each part. The radius was calculated using:

$$R = \frac{abc}{\sqrt{(a+b+c)(a+b-c)(b+c-a)(c+a-b)}}$$

where the distances between two of the three points were a, b, and c [13].

Radiographic analysis

All of the radiological assessments were performed using full-length weight-bearing AP radiographs. On taking full-length weight-bearing radiographs, each lower limb was rotated so that the knee pointed anteriorly [21]. No attempt was made to fluoroscopically control the films to avoid excessive radiation exposure.

A point was marked on each radiograph in the center of the intramedullary canal at the proximal and distal third of the femur. A line connecting these two points was defined as the femoral anatomic axis [15]. The tibial anatomic axis was found in the same manner as above. Anatomical tibiofemoral angle was determined by intersecting the femoral anatomic axis with the tibial anatomic axis [18] (Fig. 3). The lateral angle between a line tangent to both distal femoral condyles and the femoral anatomic axis or the femoral mechanical axis was defined as the femoral joint angle [17], and the hip-condylar angle, respectively (Fig. 3). The lateral angle between the tibial anatomic axis and a line parallel to the proximal articular surface was defined as the tibial joint

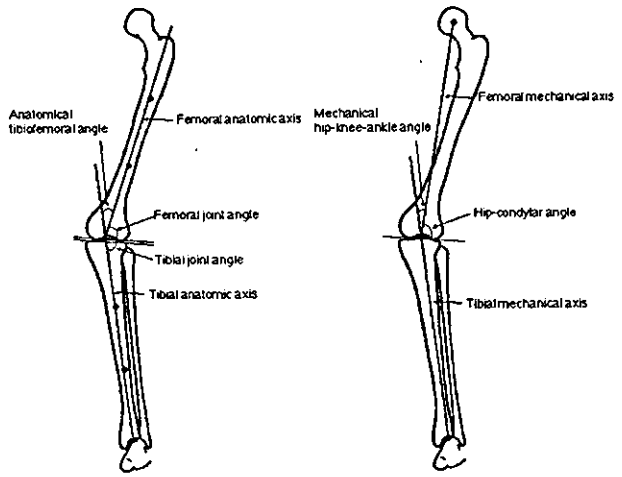

Fig. 3. The femoral anatomic axis passed two points marked in the center of the intramedullary canal of the femur, and the tibial anatomic axis passed two points marked in that of the tibia (Left). The anatomical tibiofemoral angle was created by intersecting the femoral and tibial anatomic axes. The femoral joint angle was the lateral angle between the femoral anatomic axis and a line tangent to both distal femoral condyles. The tibial joint angle was the lateral angle between the tibial anatomic axis and a line parallel to the proximal articular surface. The mechanical hip–knee–ankle angle was created by intersecting the femoral and tibial mechanical axes (Right). The femoral joint angle was the lateral angle between the femoral mechanical axis and a line tangent to both distal femoral condyles.

angle [17] (Fig. 3). The angle between the femoral mechanical axis (a line connecting hip center and knee center) and the tibial mechanical axis (a line connecting knee center and ankle center) was defined as the mechanical, hip–knee–ankle angle [6]. These radiographic parameters were compared among the normal, varus and valgus knees.

Statistical analysis was carried out using a data analysis system (StatView 5.0, Abacus Concepts, Inc., Berkeley, CA). The mean and standard deviations of all measurements were calculated. One factor analysis of variance (ANOVA) and Fisher's PLSD as the post-hoc analysis were used. P values of less than 0.05 were considered to be statistically significant.

Results

The posterior condylar tangent showed 6.4° of internal rotation in the normal knees and 6.1° in the varus knees when the angle to the transepicondylar axis was measured (Table 2, Fig. 4). However, the posterior condylar axis in the valgus knees showed 11.5° of internal rotation (Fig. 5), which was significantly larger than that in the normal and varus knees ($p < 0.0001$). The posterior condylar axis showed 6.3° of internal

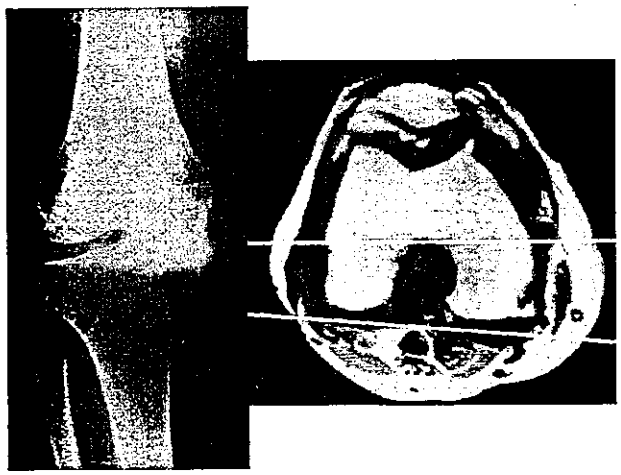

Fig. 4. Standing AP radiograph of the varus knee (Left). Magnetic resonance image of the axial view of the distal femur in the varus knee (Right). The transepicondylar axis was externally rotated 6° from the posterior condylar tangent.

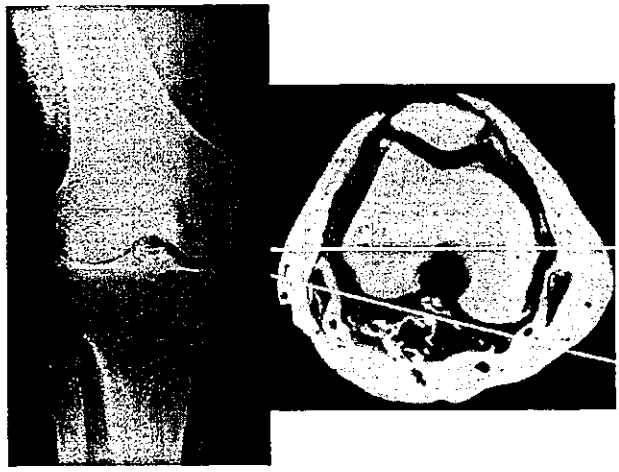

Fig. 5. Standing AP radiograph of the valgus knee (Left). Magnetic resonance image of the axial view of the distal femur in the varus knee (Right). The posterior part of the lateral condyle was relatively small compared to that of the medial condyle, and the transepicondylar axis was externally rotated 11° from the posterior condylar tangent.

Table 2
Magnetic resonance imaging analysis (axial view)

Parameter	Normal knees	Varus knees	Valgus knees
Angle between transepicondylar axis and posterior condylar tangent	6.4 ± 1.8 (3.5–10.6)	6.1 ± 1.8 (0.3–10.7)	11.5* ± 2.1 (8.1–16.9)
Angle between a line perpendicular to the anteroposterior axis and posterior condylar tangent	6.3 ± 12.4 (0.0–10.0)	6.6 ± 2.5 (3.0–12.0)	8.6* ± 2.7 (3.0–13.5)
Angle between anteroposterior axis and transepicondylar axis	90.1 ± 3.2 (84.6–100.6)	89.5 ± 2.8 (82.7–94.6)	92.9* ± 2.6 (87.0–98.0)

*Significantly different from normal knees and varus knees ($p < 0.05$).

Table 3
AP dimension of the femoral condyle

Parameter		Normal knees	Varus knees	Valgus knees
Anterior	Medial condyle	30.6 ± 3.0 (24.8–36.9)	32.4* ± 2.0 (27.9–34.8)	31.9 ± 2.1 (28.7–37.6)
	Lateral condyle	37.1 ± 4.4 (30.3–44.9)	38.3 ± 2.9 (32.7–41.9)	39.5 ± 2.5 (35.2–45.0)
Posterior	Medial condyle	29.2 ± 2.4 (25.6–34.1)	29.6 ± 2.7 (25.6–34.3)	29.9 ± 2.5 (21.6–35.4)
	Lateral condyle	24.1 ± 2.4 (20.5–30.2)	24.7 ± 2.6 (21.6–31.4)	21.9** ± 2.6 (15.6–26.9)

*Significantly different from normal knees ($p < 0.05$).
**Significantly different from normal knees and varus knees ($p < 0.05$).

Table 4
Magnetic resonance imaging analysis (sagittal view)

	Normal knee	Varus knees	Valgus knees
Medial condyle	20.3 ± 3.4 (16.1–28.0)	21.2 ± 2.1 (18.0–24.5)	21.1 ± 2.0 (17.8–24.1)
Lateral condyle	19.0 ± 3.0 (14.7–25.0)	20.8 ± 2.1 (17.5–30.0)	21.1* ± 2.1 (18.4–25.5)

*Significantly different from normal knees ($p < 0.05$).

rotation in the normal knees, 6.6° in the varus knees, and 8.6° in the valgus knees when the angle to the line perpendicular to the AP axis was measured (Table 2). The angle in the valgus knee was significantly larger than that in the normal ($p = 0.0006$) and varus knees ($p = 0.0023$). The AP axis was approximately perpendicular to the transepicondylar axis in normal and varus knees, but the AP axis was slightly internally rotated relative to the transepicondylar axis in valgus knees (Table 2).

In the measurement of the AP dimension of the anterior part of the lateral condyle, no significant difference was detected between normal, varus, and valgus knees, however the AP dimension of the medial condyle in the varus knee was significantly larger ($p = 0.0460$) than in the normal knees (Table 3). No significant difference was found in the AP dimension of the posterior part of the medial condyle between normal, varus, and valgus knees; however, the AP dimension of the lateral condyle in the valgus knee was significantly smaller than in the normal ($p = 0.0044$) and valgus knees ($p = 0.0014$) (Table 3).

Measurement of the radius of the posterior part of the medial femoral condyle did not reveal any significant differences between normal, varus, and valgus knees. The radius of the posterior part of the lateral femoral condyle in valgus knees was significantly larger ($p = 0.0384$) than the value in normal knees (Table 4, Fig. 6).

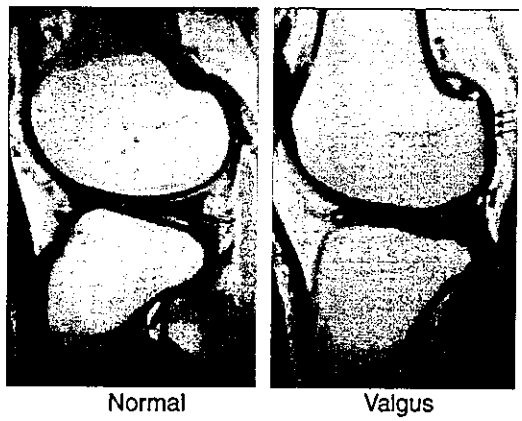

Fig. 6. Magnetic resonance image shows a sagittal view of the distal femur in a normal knee (Left). Magnetic resonance image shows a sagittal view of the distal femur in a valgus knee (Right). The posterior part of the lateral condyle is flat in shape.

In radiographic analysis, the anatomical tibiofemoral angle was 3.6° valgus in the normal knees, 5.0° varus in the varus knees, and 13.3° valgus in the valgus knees (Table 5). The patients with the varus and the valgus

Table 5
Radiographic analysis

Parameter	Normal knees	Varus knees	Valgus knees
Anatomical tibiofemoral angle	3.6 ± 2.2 (0.4–8.0)	−5.0** ± 7.0 (−30.0–6.0)	13.3* ± 4.9 (4.2–25.8)
Mechanical hip–knee–ankle angle	−1.4 ± 2.4 (−6.0 to −1.0)	−14.2** ± 5.3 (−23.0 to −6.0)	9.1* ± 6.3 (−0.7–20.8)
Femoral joint angle	83.3 ± 1.5 (80.3–85.9)	83.8 ± 2.0 (78.9–88.9)	80.7* ± 1.9 (76.7–85.0)
Hip–condylar angle	88.3 ± 2.3 (84.3–91.2)	90.4 ± 3.2 (84.9–97.0)	85.1* ± 2.3 (81.5–90.0)
Tibial joint angle	93.0 ± 1.3 (90.3–96.1)	94.3** ± 2.3 (90.1–98.6)	91.0* ± 3.2 (84.8–99.2)

*Significantly different from normal knees and varus knees ($p < 0.05$).
**Significantly different from normal knees and valgus knees ($p < 0.05$).

knees had 8.6° of varus and 9.6° of valgus deformity, respectively, compared to those with the normal knees. The mechanical, hip–knee–ankle angle was 1.4° varus in the normal knees, 14.2° varus in the varus knees, and 9.1° valgus in the valgus knees (Table 5). The femoral joint angle and the hip-condylar angle in the valgus knees was significantly smaller ($p < 0.001$) than those in the normal and varus knees (Table 5). The tibial joint angle in the valgus knees was significantly smaller than that in the normal knees ($p = 0.002$) and varus knees ($p < 0.001$), and the angle in the varus knees was significantly larger ($p = 0.032$) than that in the normal knees (Table 5).

Discussion

Proper rotational alignment of the component is one of the most important factors for successful total knee arthroplasty [1,4,14]. Previous studies recommended that the femoral component should be inserted parallel to the transepicondylar axis [5,8] or to the AP axis [3]. However, accurate detection of both the medial and lateral epicondyle is sometimes difficult [3,11], as is finding the AP axis, because of trochlear wear or intercondylar osteophytes in arthritic knees [19]. The posterior condyles can be more easily identified intraoperatively, therefore some bone cutting guide systems are designed to align the femoral component in 3–5° of external rotation from the posterior condyles. These systems align the femoral component parallel to the transepicondylar axis with a small amount of deviation, because the previous anatomical studies have shown that the transepicondylar axis is externally rotated from the posterior condylar tangent in 3–6° [2,8,9,13,22]. These anatomical studies are mainly focused on the normal or varus knees, but detailed measurement of surface geometry has not been available in valgus knees probably because valgus knee deformity is relatively rare knee condition. Griffin, et al. [8] measured the angle between the surgical epicondylar axis and the posterior condylar tangent intraoperatively and reported an average angle of 3.3° for varus knees and 5.4° for valgus knees. In that study, valgus knees were defined as knees with anatomical tibiofemoral angles greater than 7°, but the average and range of the anatomical tibiofemoral angles of the valgus knee group are unknown, and questions remain on the accuracy of intraoperative measurement. Akagi, et al. [2] measured the angle between the clinical epicondylar axis and the posterior condylar tangent as 9.1° for valgus knees and 6.4° for normal knees. However, the valgus knee group included both rheumatoid and osteoarthritis, and computed tomography evaluated the bony boundaries but not the articular boundaries of the femoral condyles. Therefore, femoral condyle geometry has not been fully evaluated in osteoarthritic knees with valgus deformity.

The results of our study showed that the posterior condylar tangent was internally rotated against the transepicondylar axis approximately 6° in both the normal and varus knees and 11.5° in the valgus knees. In performing total knee arthroplasty for a valgus knee, 3° of external rotation from the posterior condyles results in internal rotation of the femoral component relative to the transepicondylar axis by 8.5°. This amount of malrotation of the femoral component could cause patellofemoral joint complications [1,4,14]. The surgeon should take deformity of the lateral condyle into account, and the angle between the transepicondylar axis and the posterior condylar tangent should be measured using MRI (or computed tomography) before surgery. With the measured external rotational angle, easily detectable posterior condyles can be used as a reliable rotational landmark in addition to palpation of the epicondyles.

In the valgus knees, the AP dimension of the posterior part of the lateral condyle was significantly smaller than in the normal and varus knees, but the anterior part of the lateral condyle did not show a significant difference. Also in the valgus knees, we can conclude that the posterior part of the lateral condyle is relatively flat in shape based on the findings that the radius of the posterior arc of the lateral femoral condyle was significantly larger than in the normal knees. These findings suggest that the posterior part of the lateral condyle in the valgus knees is distorted, but there is no hypoplasia in the posterior part of the medial condyle in the varus knees. Therefore, distorted posterior condyles are the main mechanism causing the posterior condylar tangent to be more internally rotated in the valgus knees than in the normal and varus knees, relative to the transepicondylar axis. The AP dimension of the anterior part of the medial condyle in the varus knees was larger than in the normal knees, probably due to osteoarthritic changes of the anterior condyles.

The results of this study also showed that the AP axis was approximately perpendicular to the transepicondylar axis in normal and varus knees, but slightly internally rotated in valgus knees. We cannot conclude which landmark should be used in valgus knees from our results; however, these results suggest that the AP axis measurements might deviate due to distorted arthritic articular geometry.

The results of the coronal plane (radiographic) analysis showed that the femoral joint angle in the valgus knees was significantly smaller than that in the varus and the normal knees, but no significant difference was detected between the varus knees and the normal knees. These results suggests that hypoplasia was not present in the distal part of the medial condyle in the varus knees, but the distal part of the lateral condyle in the valgus knees was distorted, as well as the posterior part of the lateral condyle, although the difference detected was

more distinct in the posterior part. It was unclear whether the distorted lateral condyle in the valgus knees was the factor contributing to osteoarthritis of the lateral compartment of the knee or was a result of the valgus deformity. A significant difference in the distal femur geometry was detected between the normal and valgus knees, but not detected between the normal and varus knees, even though patients with the varus knees had the same degree of knee deformity as those with the valgus knees in anatomical tibiofemoral angle. Therefore, we could say that osseous abnormality of the femur contributed to the knee deformity more predominantly in valgus knees than in varus knees. From the findings of this study, however, we are unable to conclude that the distorted lateral femoral condyle caused osteoarthritis of the lateral compartment.

The tibial joint angle in the normal knees was significantly smaller than that in the varus knees and significantly larger than that in the valgus knees, suggesting that osseous abnormality of the tibia exists in both the varus and valgus knees and that the tibial deformity is the contributing factor to the overall malalignment of the leg. Both the varus and valgus knees had lowered tibial plateau in the affected compartment compared to the normal knees, suggesting that osseous abnormality of the tibia was possibly caused by degenerative changes of osteoarthritis rather than by developmental abnormality.

The current study has some limitation. Better matching of the groups in terms of gender and age may have strengthened the study. It was difficult, however, to do this because valgus knee deformity is a relatively rare knee condition. Many studies have shown that no marked difference is present in femoral condyle geometry between male and female [8,9,19,23]. Therefore, we believe the heavy preponderance of females in our valgus knee group did not significantly affect our results. In addition, all of the anatomic specimens in the current study were Japanese; therefore, these findings may not apply to other racial groups.

In summary, radiographic and MRI analysis showed that hypoplasia of the lateral condyle existed in the valgus knees, but not in the medial condyle in the varus knee. In total knee arthroplasty for valgus knee, the extent of hypoplasia of the lateral condyle should be evaluated preoperatively to achieve the correct rotational alignment.

References

[1] Akagi M, Matsusue Y, Mata T, et al. Effect of rotational alignment on patellar tracking in total knee arthroplasty. Clin Orthop 1999;366:155–63.

[2] Akagi M, Yamashita E, Nakagawa T, et al. Relationship between frontal knee alignment and reference axes in the distal femur. Clin Orthop 2001;388:147–56.

[3] Arima J, Whiteside LA, McCarthy DS, White SE. Femoral rotational alignment, based on the anteroposterior axis, in total knee arthroplasty in a valgus knee. J Bone Joint Surg [Am] 1995;77:1331–4.

[4] Berger RA, Crossett LS, Jacobs JJ, Rubash HE. Malrotation causing patellofemoral complications after total knee arthroplasty. Clin Orthop 1998;356:144–53.

[5] Berger RA, Rubash HE, Seel MJ, et al. Determining the rotational alignment of the femoral component in total knee arthroplasty using the epicondylar axis. Clin Orthop 1993;286: 40–7.

[6] Cooke D, Scudamore A, Li J, et al. Axial lower-limb alignment: comparison of knee geometry in normal volunteers and osteoarthritis patients. Osteoarthr Cartilage 1997;5:39–47.

[7] Elias SG, Freeman MAR, Gokcay EI. A correlative study of the geometry and anatomy of the distal femur. Clin Orthop 1990; 260:98–103.

[8] Griffin FM, Insall JN, Scuderi GR. The posterior condylar angle in osteoarthritic knees. J Arthroplasty 1988;12:812–5.

[9] Griffin FM, Math K, Scuderi GR, et al. Anatomy of the epicondyles of the distal femur. MRI analysis of normal knees. J Arthroplasty 2000;15:354–9.

[10] Hollister AM, Jatana S, Singh AK, et al. The axes of rotation of the knee. Clin Orthop 1993;290:259–68.

[11] Katz MA, Beck TD, Silber JS, et al. Determining femoral rotational alignment in total knee arthroplasty: reliability of techniques. J Arthroplasty 2001;16:301–5.

[12] Kurosawa H, Walker PS, Garg A, Hunter T. Geometry and motion of the knee for implant and orthotic design. J Biomech 1985;18:487–99.

[13] Matsuda S, Matsuda H, Miyagi T, et al. Femoral condyle geometry in the normal and varus knee. Clin Orthop 1998; 349:183–8.

[14] Matsuda S, Miura H, Nagamine R, et al. Effect of the femoral and tibial component position on patellar tracking following total knee arthroplasty. 10-year follow-up of Miller Galante I knees. Am J Knee Surg 2001;14:152–6.

[15] Moreland JR, Bassett LW, Hanker GJ. Radiographic analysis of the axial alignment of the lower extremity. J Bone Joint Surg [Br] 1987;69:745–9.

[16] Murray PB, Rand JA. Symptomatic valgus knee: the surgical options. J Am Acad Orthop 1993;1:1–9.

[17] Nagamine R, Miura H, Bravo CV, et al. Anatomic variations should be considered in total knee arthroplasty. J Orthop Sci 2000;5:232–7.

[18] Petersen TL, Engh GA. Radiographic assessment of knee alignment after total knee arthroplasty. J Arthroplasty 1988;3:67–72.

[19] Poilvache PL, Insall JN, Scuderi GR, Font-Rodriguez DE. Rotational landmarks and sizing of the distal femur in total knee arthroplasty. Clin Orthop 1996;331:35–46.

[20] Phillips MJ, Krackow KA. Distal femoral varus osteotomy. Indications and surgical technique. Inst Course Lec 1999;48: 125–9.

[21] Siu D, Cooke TDV, Brokenhoven LD, et al. A standardized technique for lower limb radiography: practice, applications, and error analysis. Invest Radiol 1991;26:71–7.

[22] Yoshino N, Takai S, Ohtsuki Y, Hirasawa Y. Computed tomography measurement of the surgical and clinical transepicondylar axis of the distal femur in osteoarthritic knees. J Arthroplasty 2001;16:493–7.

[23] Yoshioka Y, Siu D, Cooke TDV. The anatomy and functional axes of the femur. J Bone Joint Surg [Am] 1987 69:873–80.

Cell-based Protein Delivery System for the Inhibition of the Growth of Pancreatic Cancer: NK4 Gene-transduced Oral Mucosal Epithelial Cell Sheet[1]

Tatsuya Manabe,[2] Kazuhiro Mizumoto, Eishi Nagai, Kunio Matsumoto, Toshikazu Nakamura, Toshihiro Nukiwa, Masao Tanaka, and Takehisa Matsuda

Divisions of Biomedical Engineering [T. Man., T. Mat.] and Surgery and Oncology [T. Man., K. Mi., E. N., M. T.], Graduate School of Medicine, Kyushu University, Maidashi, Fukuoka 812-8582; Division of Molecular Regenerative Medicine, Course of Advanced Medicine, Osaka University Graduate School of Medicine, Suita, Osaka 565-0871 [K. Ma., T. Na.]; and Division of Respiratory Oncology and Molecular Medicine, Institute of Development, Aging and Cancer, Tohoku University, Sendai 980-8575 [T. Nu.], Japan

ABSTRACT

Purpose: **Pancreatic resection for pancreatic cancer is the only curative modality, but the high incidence of local recurrence after surgery results in a very poor prognosis. This study aims to develop a new therapeutic tool that could inhibit the growth of remnant cancer cells, which is based on local delivery of NK4 (hepatocyte growth factor antagonist) secreted from an *NK4* gene-transduced oral mucosal epithelial cell (OMEC) sheet (NK4-sheet), which is adhered to the resected surface.**

Experimental design: **OMECs, harvested and cultured according to 3T3 feeder layer technique, were seeded on a collagen mesh-overlayered, biodegradable VICRYL mesh to produce an OMEC sheet. *NK4* gene transduction was mediated by recombinant adenovirus (Ad-NK4). Applicability of OMECs for cell-based NK4 delivery was examined. An experimental model using nude mice was established to determine the effect of an NK4-sheet on both tumor growth and angiogenesis.**

Results: **NK4 secreted from Ad-NK4-transduced OMECs suppressed MRC-5-induced invasion of pancreatic cancer cell lines. Heterotopically implanted gene-transduced OMECs remained for ≥10 days while gradually decreasing. NK4-sheets inhibited both angiogenesis and tumor growth *in vivo*.**

Conclusion: **Autologous OMEC was found to be suited to this purpose because of no secretion of hepatocyte growth factor, ease in harvesting from a patient, reasonably high proliferation potential, and no immune reaction. Although NK4-sheets under development exhibited a low level and short period of NK4 secretion, it is expected that this system may have a great potentiality of protein delivery system to target tissue at clinical situations when it is loaded with multilayered OMECs.**

INTRODUCTION

Pancreatic cancer remains difficult to cure, and pancreatic resection is the only curative modality. Pancreatic cancer, even if small, often invades surrounding tissues and induces local recurrence after surgery at a high incidence, resulting in a very poor prognosis (1, 2). Although some adjuvant therapies, such as intraoperative radiotherapy and adjuvant chemotherapy, have been tested, satisfactory results have not been obtained as yet. Therefore, development of a new therapeutic modality to prevent the local recurrence has been awaited.

The local recurrence after pancreatic resection is generally caused by the high migratory and invasive potentials of pancreatic cancer cells. Such malignant behavior is usually affected by many kinds of cytokines. HGF[3] is known to act as a potent scattering factor by binding to c-Met receptor expressed on cells (3, 4). HGF antagonist, NK4, composed of the NH_2-terminal hairpin and four kringle domains of the α-subunit of HGF, binds to the c-Met receptor but does not induce tyrosine phosphorylation of c-Met, resulting in inhibition of mitogenic, motogenic, and morphogenic activities of HGF (5, 6). Recent studies showed that NK4 inhibits growth and migration of vascular endothelial cells stimulated by angiogenic growth factors (7, 8) and that the c-Met receptor is frequently overexpressed in pancreatic cancers (9–11). NK4 injection to a tumor and NK4-encoding adenovirus-mediated gene transduction suppressed the migration, invasion, and growth of pancreatic cancer cells *in vitro* and *in vivo* (9, 12–15).

In our previous study, we developed a local delivery system of a protein and an adenoviral vector using *in situ* photocured gelatin: a bioactive substance-immobilized, tissue-adhesive matrix (16, 17). Protein delivery from photocured gelatin adhered to a living tissue proceeded with time. However, the

Received 12/17/02; revised 3/20/03; accepted 3/26/03.
The costs of publication of this article were defrayed in part by the payment of page charges. This article must therefore be hereby marked *advertisement* in accordance with 18 U.S.C. Section 1734 solely to indicate this fact.
[1] Supported by Promotion Fundamental Studies in Health Science of the Organization for Pharmaceutical Safety and Research (contract Grant 97-15) and Grant-in-Aid for Scientific Research from Ministry of Education, Culture, Sports, Science and Technology, Japan (contract Grants A2-12358017 and B2-12470277).
[2] To whom requests for reprints should be addressed, at Division of Biomedical Engineering, Graduate School of Medicine, Kyushu University, 3-1-1 Maidashi, Fukuoka 812-8582, Japan. Phone: 81-92-642-6211; Fax: 81-92-642-6212; E-mail: manabe@med.kyushu-u.ac.jp.

[3] The abbreviations used are: HGF, hepatocyte growth factor; OMEC, oral mucosal epithelial cell; SEM, scanning electron microscopy; MOI, multiplicity of infection; FBS, fetal bovine serum; RT-PCR, reverse transcription-PCR.